Batteries & Supercaps

Research Article
doi.org/10.1002/batt.202500296

Chemistry Europe
European Chemical Societies Publishing

www.batteries-supercaps.org

# Promoting the Energy Conversion of Li–$CO_2$/$O_2$ Batteries via Ru-Doped HKUST with Substantial Adsorption and Excellent Catalytic Effect

Ke Li, Ningning Zhu, Xueqi Tan, Xuechun Li, Yifan Xu, Enyi Zhang, Ziqiang Bi, Jou-Hyeon Ahn, Sheng Ju,* and Xiaohui Zhao*

Li–$CO_2$/$O_2$ batteries hold tremendous promises for energy storage and conversion systems, attributed to their high theoretical energy density and economic viability. Nevertheless, their widespread application is hindered by high overpotential and compromised cycling stability. Herein, ruthenium (Ru)-doped copper-based metal organic frameworks (HKUST) octahedral particles (Ru@HKUST) are synthesized as the cathode catalyst for Li–$CO_2$/$O_2$ batteries. The Ru@HKUST matrix rich in free channels provides unimpeded gas permeation and substantial adsorption spaces for $CO_2$/$O_2$. A synergistic interaction between HKUST and Ru significantly enhances the kinetic conversion of $Li_2CO_3$ upon cycles, thereby markedly boosting the capacity and extending the cycle life of Li–$CO_2$/$O_2$ batteries. A high discharge capacity of 19 437 mAh $g^{-1}$ is achieved at 2 V cutoff voltage in the Li–$CO_2$/$O_2$ cell with Ru@HKUST under a constant current density of 200 mA $g^{-1}$. The cells exhibit a superior catalytic efficiency with reduced charge plateaus of 4.1 V for over 100 cycles at a fixed capacity of 1000 mAh $g^{-1}$, demonstrating excellent electrochemical properties and paving the way for advanced battery technology.

## 1. Introduction

The finite reserves and ongoing exploitation of fossil fuels have led to their gradual depletion and impending exhaustion. Furthermore, the misuse of these fuels has caused significant environmental challenges, including global warming, excessive $CO_2$ emissions, and rising sea levels. Consequently, there is an urgent need to explore alternative and environmentally friendly energy sources to address the current energy crisis.[1] One promising solution is the introduction of $CO_2$ into the Lithium–Air battery system, utilizing $CO_2$ as a renewable energy carrier for further fixation and conversion.[2] Moreover, $CO_2$-based batteries are particularly valuable in specific circumstances, such as underwater or on Mars, offering new energy solutions for human exploration endeavors.

Utilizing atmospheric $CO_2$ as the cathodic active material aligns with carbon neutrality goals by eliminating the need for specialized energy storage. However, several challenges remain in practical applications. The slow and irreversible three-phase reactions at the cathode complicate the utilization of active mass and efficient energy conversion. Besides, the electrolyte decomposition and irreversible electrochemical reactions during charge and discharge cycles passivate the cathode surface with inert lithium carbonate ($Li_2CO_3$).[3–5] Additionally, the instability of the air cathode leads to low reaction kinetics and poor cycling stability. Achieving high-performance Li–$CO_2$ batteries necessitates the exploration of efficient catalysts.[6,7] It is imperative to design a reasonable and efficient cathode catalyst that can effectively decompose $Li_2CO_3$ with low charging overpotential (usually higher than 4.3 V vs $Li/Li^+$), which fundamentally leads to a decrease in the reversible cycling life of Li–$CO_2$ batteries.[8,9] Zhou et al. found that $Li_2CO_3$ can be reversibly decomposed during the charging process of Li–$CO_2$/$O_2$ batteries.[10] Qiao et al. used ruthenium (Ru) as a catalyst to explore the decomposition mechanism of $Li_2CO_3$ and observed a reduction in the charging voltage of the battery to ≈3.6 V.[11] They also observed the simultaneous reduction of $Li_2CO_3$ and C during charging, from which they inferred the co-electrolysis pathway of $Li_2CO_3$ and C. Wang et al. coated Ru nanosheets uniformly on nickel foam (Ru/Ni) to improve active sites for the decomposition of $Li_2CO_3$ during charging and promote the decomposition kinetics of $Li_2CO_3$.[12–14] The intrinsic half-filled antibonding state of noble metals can provide the catalyst with appropriate adsorption, thus improving reaction kinetics.[15] Furthermore, Ru not only exhibits electrochemical stability but also possesses unfilled d-electron orbitals, allowing it to reversibly change its oxidation state and form intermediate products with lower activation energy, thereby

K. Li, N. Zhu, X. Tan, X. Li, Y. Xu, E. Zhang, Z. Bi, S. Ju, X. Zhao
School of Optical and Electronic Information
Jiangsu/Suzhou Key Laboratory of Biophotonics and International Joint Metacenter for Advanced Photonics and Electronics
Suzhou City University
Suzhou 215104, China
E-mail: shengju@szcu.edu.cn
zhaoxh@szcu.edu.cn

K. Li, N. Zhu, X. Tan
College of Energy
College of Physics Science
Soochow University
Suzhou 215006, China

J.-H. Ahn
Department of Materials Engineering and Convergence Technology
Gyeongsang National University
Jinju 52828, Korea

Supporting information for this article is available on the WWW under https://doi.org/10.1002/batt.202500296

Research Article
doi.org/10.1002/batt.202500296
Chemistry Europe
European Chemical Societies Publishing

reducing the charging voltage of Li–$CO_2$/$O_2$ batteries. This avoids the decomposition of organic electrolytes, ultimately improving energy conversion efficiency and optimizing cycling performance.[16–19]

Although noble metal catalysts have enhanced energy conversion in comparison with pure carbon-based materials, the irreversible electrochemical decomposition of the discharge product $Li_2CO_3$ during charging, coupled with carbon accumulation, leads to cathode surface passivation and significantly reduces catalyst activity.[20] To address this issue, we employed a porous material to enhance gas diffusion efficiency. In this work, a copper-based metal organic frameworks (HKUST) doped with ruthenium was synthesized as the cathode catalyst for Li–$CO_2$/$O_2$ batteries.[21,22] The Ru doping generated efficient catalytic active sites for reaction kinetics, while the abundant pores in the HKUST framework provided strong gas adsorption via sufficient diffusion channels for reactant gases and electrolytes. Also, its high specific surface area facilitated extensive exposure of reaction sites, further accelerating the gas diffusion and reaction kinetics.[23,24]

## 2. Results and Discussion

A solvothermal synthesis was employed to ensure the uniform dispersion of Ru within the HKUST framework. The crystal phase and structural characteristics of the synthesized HKUST and Ru@HKUST materials were analyzed using X-ray diffraction (XRD). The XRD pattern of HKUST displayed three distinct diffraction peaks at $2\theta = 6.7°$, 9.6°, and 11.7°, corresponding to the (200), (220), and (222) planes of the HKUST structure (**Figure 1**a).[25] These peaks match perfectly with the simulated XRD spectrum of HKUST, confirming the successful synthesis of the framework. The XRD pattern of Ru@HKUST exhibited the same characteristic peaks as HKUST without distinct diffraction peaks for Ru or $RuO_x$ observed, indicating that the crystal structure of HKUST was preserved after Ru doping.[26,27] The inductively coupled plasma spectrometry (ICP) results confirmed the successful incorporation of Ru into the HKUST structure, with concentrations of Cu and Ru found to be 53.3 mg $L^{-1}$ and 16.1 mg $L^{-1}$, respectively (Table S1, Supporting Information); thus, the mass fractions of Cu and Ru were calculated to be 26.7% and 8.1%, respectively. This yields a molar ratio of Cu to Ru of 3.7:1.

The Brunauer–Emmett–Teller (BET) results for HKUST and Ru@HKUST under $CO_2$ atmosphere (Figure 1b) revealed that HKUST exhibited excellent $CO_2$ adsorption capacity. At a pressure below 400 mmHg, Ru@HKUST showed higher $CO_2$ adsorption than HKUST, which is attributed to the enhanced $CO_2$ affinity of HKUST after Ru doping.[28] As pressure increased over 400 mmHg, the $CO_2$ adsorption capacity of HKUST exceeded that of Ru@HKUST. For instance, at a $CO_2$ pressure of 778 mmHg ($P_0 \approx 760$ mmHg), HKUST adsorbed about 70.4 $cm^3\,g^{-1}$ $CO_2$, while Ru@HKUST adsorbed ≈55.8 $cm^3\,g^{-1}$ $CO_2$. It is indicated that a trace of $RuO_x$ may occupy partial free space in Ru@HKUST and lead to a lower overall $CO_2$ adsorption capacity.[29]

The scanning electron microscope (SEM) was employed further to investigate the morphologies and structures of

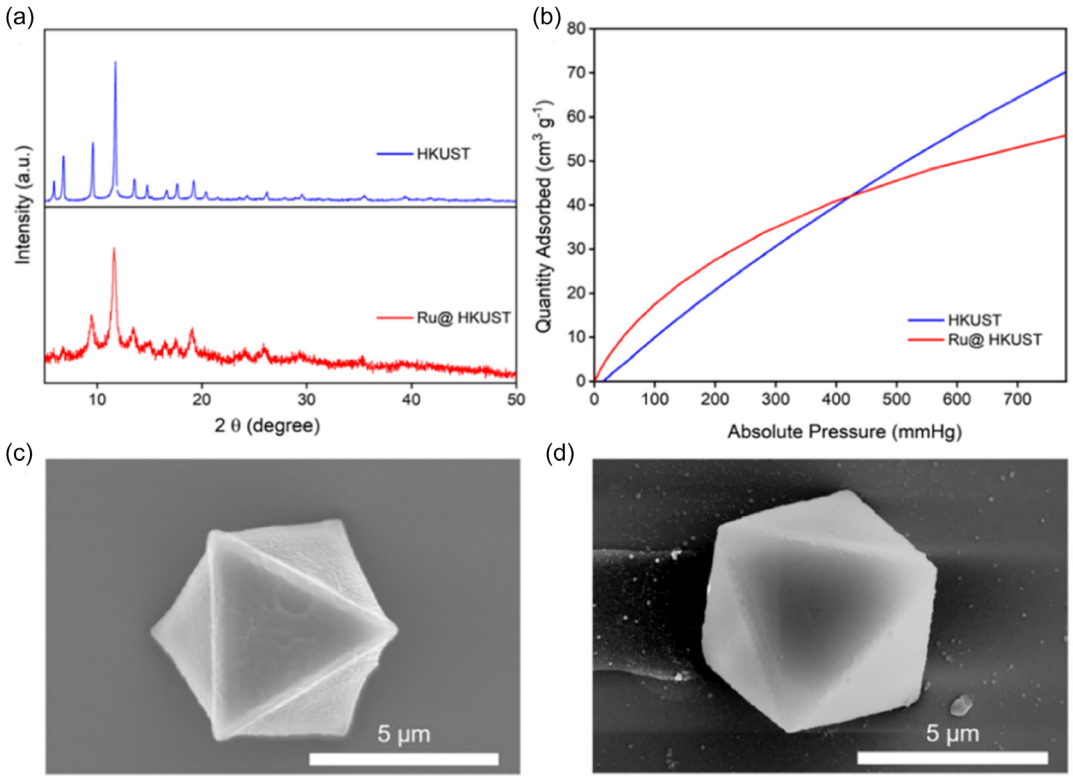


**Figure 1.** The structure and morphology of HKUST and Ru@HKUST: a) XRD patterns and b) BET plot under $CO_2$ atmosphere; SEM images of c) HKUST and d) Ru@HKUST.

HKUST and Ru@HKUST. The SEM images showed that both materials exhibited a regular octahedral morphology. The average particle size of HKUST was ≈6.5 μm (Figure 1c), and it increased slightly to about 6.7 μm with Ru doping in Ru@HKUST (Figure 1d). This indicated that the doping of Ru did not alter the octahedral morphology of HKUST. This preservation would be beneficial for the diffusion of electrolytes and $CO_2/O_2$ gases and for accommodating the deposition of $Li_2CO_3$ on the cathode.[30]

The morphologies and structures of the Ru catalyst were further characterized with high-resolution transmission electron microscopy transmission electron microscopy (TEM) (**Figure 2**). The uniform particle morphology full of pores inside is observed in Figure 2a and dispersed pores are found in the Ru@HKUST matrix (Figure 2b), confirming the successful synthesis of HKUST. The homogenous distribution of C, Ru, and Cu elements with no significant particle aggregation was verified via the high - angle annular dark field (HADDF) and energy dispersive spectroscope (EDS) mapping (Figure 2c–f). The well-doped Ru in HKUST indicated that the synthesis method effectively prevents agglomeration. This homogeneous distribution would facilitate the maximization of catalytic active sites, promote $CO_2$ reduction, and reduce the charge-discharge overpotential.

The X-ray photoelectron spectroscopy (XPS) was used to analyze the surface chemical states of HKUST and Ru@HKUST materials, focusing on the elemental composition and oxidation states. The survey spectra of Ru@HKUST confirmed the coexistence of C, O, Cu, and Ru in the composite (Figure S1, Supporting Information). High-resolution XPS spectra are shown in **Figure 3**. The C 1*s* spectrum for HKUST and the combined Ru 3*d* + C 1*s* spectrum for Ru@HKUST are shown in Figure 3a. In the C 1*s* spectrum, the peak at 284.8 eV corresponded to C—C single bonds, 285.8 eV to O—C═O and C═O bonds, and 288.7 eV to C═O double bonds. The C—C/C═C and O—C═O bonds were associated with HKUST ligands, while the C═O bonds may result from minor surface oxidation or adsorbed $CO_2$.[31] For Ru@HKUST, in addition to the above peaks, signals at 282.4 and 286.7 eV were observed, corresponding to Ru oxidation states in the Ru 3*d* spectrum.[32] In the O 1*s* spectrum (Figure 3b), the peaks at 531.8 eV were assigned to O—C═O bonds, and the peak at 532.8 eV was attributed to C═O bonds, consistent with the C 1*s* spectrum.[33] Additionally, Ru@HKUST showed an extra peak at 532.6 eV, suggesting the existence of Ru—O bonds.[34,35] Figure 3c presents the Ru 3*p* spectrum in Ru@HKUST, where peaks at 464.3 and 486.3 eV corresponded to Ru $3p_{3/2}$ and Ru $3p_{1/2}$, respectively, indicating that Ru was in an oxidized state, but not reaching the +4 oxidation state.[36] It implied that Ru was bonded via O and doped in the crystal structure of HKUST. In the Cu 2*p* spectra (Figure 3d), peaks at 933.1 and 952.5 eV were attributed to $Cu^+$ $2p_{3/2}$ and $Cu^+$ $2p_{1/2}$, respectively, while peaks at 935.3 and 954.7 eV corresponded to $Cu^{2+}$ $2p_{3/2}$ and $Cu^{2+}$ $2p_{1/2}$, respectively. It was noted that the content of $Cu^+$ was increased after Ru doping, indicating that the Cu valence state in HKUST was by Ru substitution.[37]

HKUST and Ru@HKUST were evaluated as cathode catalysts in Li–$CO_2/O_2$ batteries under a $CO_2/O_2$ atmosphere with a 9:1 ratio. **Figure 4**a illustrates the cycle voltammetry (CV) curves of Li–$CO_2/O_2$ cells with HKUST and Ru@HKUST. During discharge, Ru@HKUST displayed a reduction peak at 2.7 V, whereas HKUST showed a reduction peak at 2.3 V, suggesting an improved

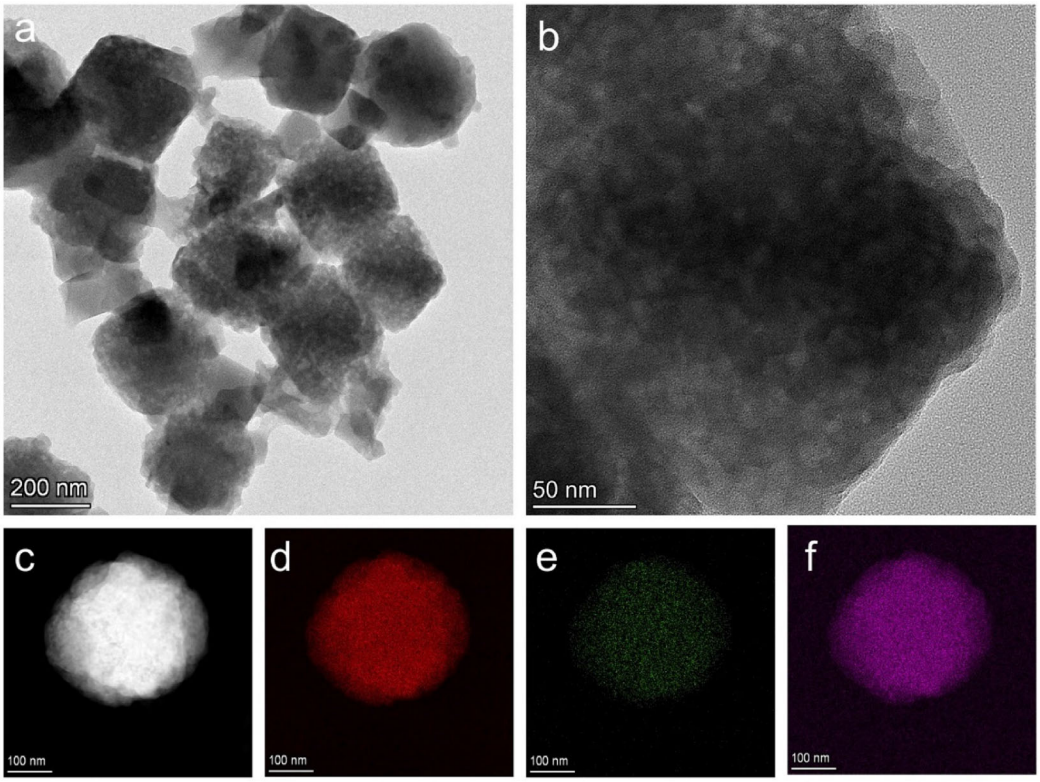


**Figure 2.** a,b) TEM images and c) HADDF and EDS elemental mapping of d) C, e) Ru, and f) Cu of Ru@HKUST.

Research Article
doi.org/10.1002/batt.202500296
Chemistry Europe
European Chemical Societies Publishing

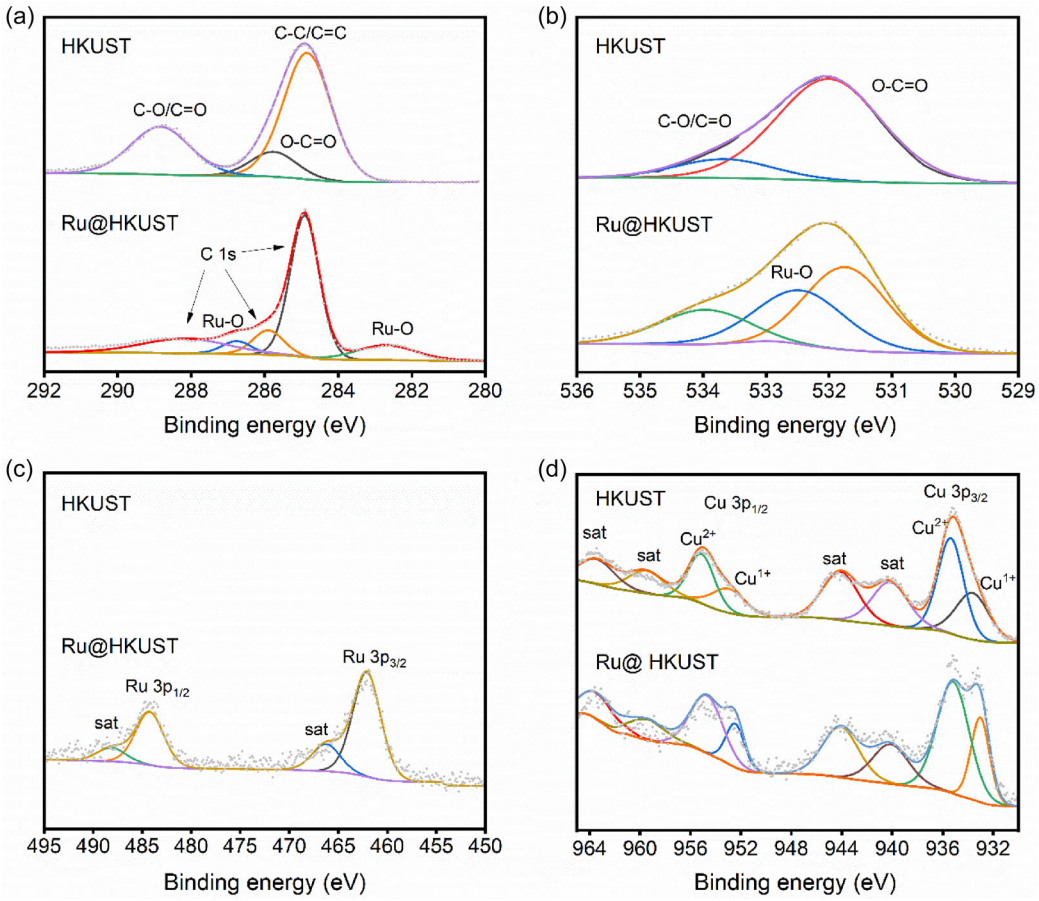


**Figure 3.** XPS spectra of HKUST and Ru@HKUST: a) Ru 3*d* + C 1*s*, b) O 1*s*, c) Ru 3*p*, and d) Cu 2*p*.

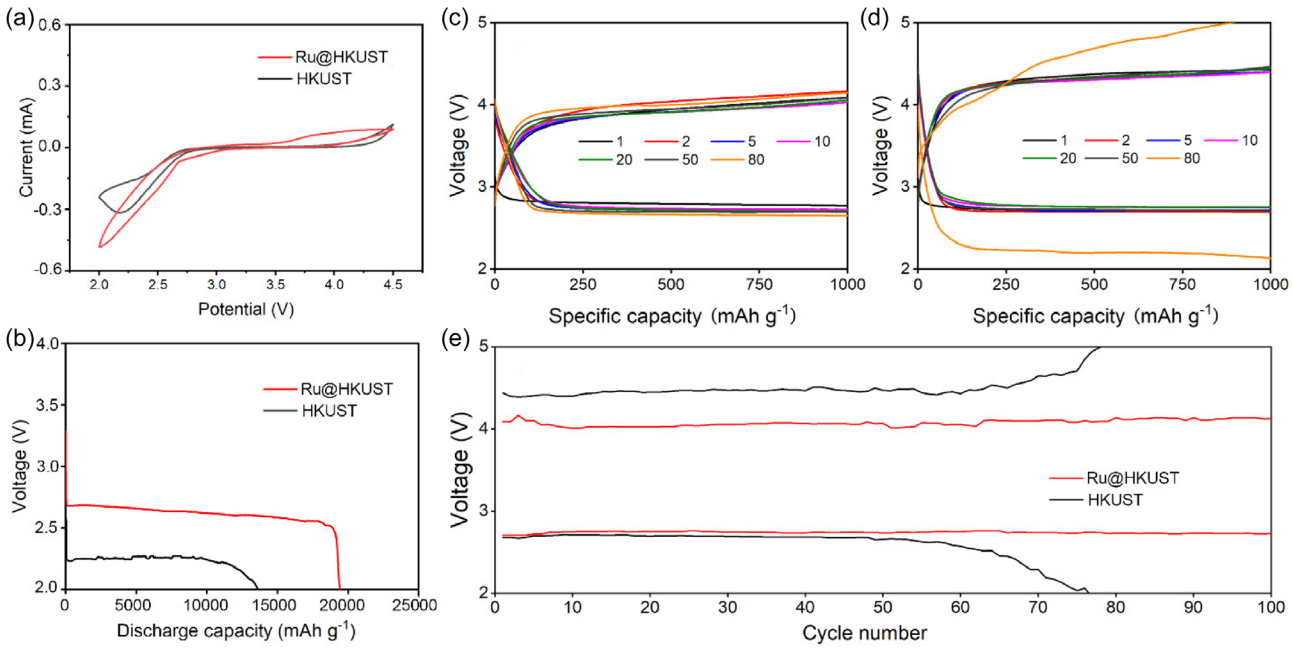


**Figure 4.** The electrochemical performances of Li–$CO_2$/$O_2$ batteries with HKUST and Ru@HKUST catalysts: a) CV curves, b) discharge performance at a current density of 200 mA $g^{-1}$, c,d) the charge–discharge profiles at a current density of 200 mA $g^{-1}$, and e) the corresponding voltage plateau changes in 100 cycles.

capacity and lowered for polarization for Ru@HKUST with a Ru-enhanced $CO_2$ reduction process.[38,39]

Upon charging, Ru@HKUST exhibited an oxidation peak at 3.7 V, and HKUST, however, showed an oxidation peak at around 4.3 V, demonstrating that Ru incorporation significantly lowered the decomposition potential of $Li_2CO_3$.[40] Figure 4b shows the discharge performance of Ru@HKUST and HKUST at a current density of 200 mA $g^{-1}$. Both batteries were discharged to 2.0 V, with Ru@HKUST achieving a discharge capacity of 19 437 mAh $g^{-1}$, compared to a lower value of 13 578 mAh $g^{-1}$ for HKUST. The discharge plateaus were 2.6 V for Ru@HKUST and 2.3 V for HKUST. The higher specific capacity and lower discharge voltage of Ru@HKUST were primarily credited to the effective catalytic action of Ru doping, accelerating the discharge reaction rate and enhancing the energy conversion efficiency.[41] The interaction of Ru—O active sites facilitated the deposition of $Li_2CO_3$ on the electrode, preventing obstructive accumulation that impeded electron and ion conduction as well as gas diffusion.[42]

To evaluate the catalytic performance of Ru@HKUST and HKUST, cycle performance tests on both cathode materials with a cutoff capacity of 1000 mAh $g^{-1}$ were conducted. For Ru@HKUST, the charge and discharge voltages were 4.1 and 2.8 V, respectively, when the charge and discharge capacities reached 1000 mAh $g^{-1}$ (Figure 4c), while HKUST exhibited higher charge voltages of 4.4 V under the same conditions (Figure 4d). Although HKUST excelled in adsorbing more gas, it lacked catalytic activity for the decomposition of $Li_2CO_3$, resulting in a higher charge plateau.[43,44] In contrast, Ru@HKUST facilitated the decomposition of $Li_2CO_3$ owing to the Ru—O active sites with a low polarization. It is noted that the cycle performance of Ru@HKUST remained stable over the first 100 cycles with low polarization, demonstrating excellent electrochemical performance and stability of the Li–$CO_2$/$O_2$ batteries (Figure 4e). The uniformly distributed ruthenium may suppress the irreversible accumulation of $Li_2CO_3$, thereby prolonging the cycle life.

Moreover, the lower resistance of the Ru@HKUST cell (49.5 Ω) compared to that of HKUST (134.5 Ω) as shown in the electrochemical impedance spectroscopy plots revealed its rapid electrochemical kinetics (Figure S2, Supporting Information).

The performance discrepancy became more pronounced at higher current densities. For instance, at 500 mA $g^{-1}$, Ru@HKUST exhibited initial charge and discharge voltages of 4.4 and 2.7 V, respectively (Figure S3a, Supporting Information). By the 200th cycle, these voltages increased to 4.6 and 2.5 V. Nevertheless, The $CO_2$/$O_2$ cell with HKUST catalyst displayed much lower discharge voltage (2.1 V) and higher charge voltage (4.9 V) in the 200th cycle (Figure S3b, Supporting Information). Probably, the incomplete $CO_2$/$O_2$ dissolution within the cell leads to higher discharge voltage.[45] Without the catalytic effect of Ru—O, $Li_2CO_3$ decomposition was insufficient, resulting in the accumulation of insulating $Li_2CO_3$ on the electrode surface. This reduced electrode conductivity and blocked HKUST pores, impeding $CO_2$/$O_2$ and electrolyte diffusion. When the voltage exceeds 4.5 V, electrolyte decomposition accelerates, further diminishing the battery life. Besides, the cell with Ru@HKUST showed smaller voltage gap between discharge and charge (Figure S3c, Supporting Information). Therefore, Ru@HKUST acts as an effective bifunctional catalyst with reduced overpotentials.[46]

The density functional theory (DFT) calculation further emphasized the superior catalytic effect of Ru@HKUST owing to its stronger adsorption to $LiCO_3$ with a higher binding of energy −1.94 eV compared to that of HKUST (**Figure 5** and S4, Supporting Information), which enhanced the deposition and decomposition of $Li_2CO_3$, ensuring more complete $CO_2$/$O_2$ reduction and minimizing side reactions associated with electrolyte degradation. This unique feature not only enhances the catalytic activity but also provides abundant active sites, facilitates reactant accessibility, and thereby accelerates the decomposition of $Li_2CO_3$.

## 3. Conclusion

In summary, a Ru@HKUST catalyst has been successfully developed for Li–$CO_2$/$O_2$ batteries. The 3D regular pore structure of HKUST facilitates $CO_2$ gas diffusion and ensures efficient decomposition during charging, thereby enhancing reaction kinetics. The Ru—O bonds formed in HKUST created excess active sites for the efficient transformation of $Li_2CO_3$ and $CO_2$/$O_2$, thus facilitating the reaction kinetics in the Li–$CO_2$/$O_2$ batteries. At a constant current density of 200 mA $g^{-1}$ and a fixed cutoff capacity of 1000 mAh $g^{-1}$, the cells with Ru@HKUST maintained charge and discharge potentials of 4.1 and 2.8 V, respectively, demonstrating lower polarization in the batteries. Furthermore, Ru@HKUST exhibits effective catalytic activity that enhances $Li_2CO_3$ decomposition during charging and minimized electrolyte decomposition within the operational potential range of the Li–$CO_2$/$O_2$

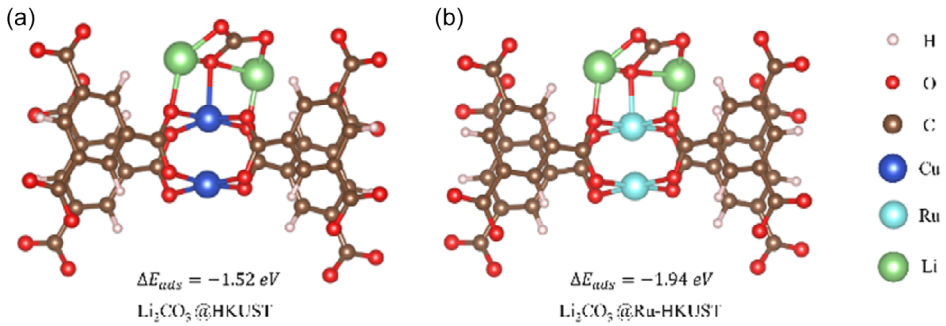


**Figure 5.** DFT calculations for optimized $Li_2CO_3$ adsorption configurations and adsorption energies on the surface of a) HKUST and b) Ru@HKUST.

batteries, demonstrating the promising potential for its further applications in $CO_2$-based batteries.

## Acknowledgements

This work was financially supported by 2023 QINGLAN Project of Jiangsu Province of China, International Talent Cultivation Brand Program in New Energy Materials and Devices of Suzhou City University, Suzhou Basic Research Project (grant no. SJC2023003), National College Students' Innovation and Entrepreneurship Training Program (grant nos. 202413983016Z and 202413983023Z), and Jiangsu Provincial College Students' Innovation and Entrepreneurship Training Program (grant no. 202413983085Y).

## Conflict of Interest

The authors declare no conflict of interest.

## Author Contributions

**Ke Li**: methodology (lead); writing—original draft (lead). **Ningning Zhu**: formal analysis (lead). **Xueqi Tan**: investigation (supporting). **Xuechun Li**: investigation (supporting). **Yifan Xu**: investigation (supporting). **Enyi Zhang**: investigation (supporting). **Ziqinag Bi**: investigation (supporting). **Jou-Hyeon Ahem**: project administration (supporting). **Sheng Ju**: formal analysis (lead); supervision (equal). **Xiaohui Zhao**: conceptualization (lead); funding acquisition (lead); project administration (lead); supervision (lead); writing—review and editing (lead). **Ke Li** and **Ningning Zhu** contributed equally to this work.

## Data Availability Statement

Research data are not shared.

**Keywords:** HKUST · $Li_2CO_3$ · Li–$CO_2$/$O_2$ batteries · Ru

[1] S. Xie, K. Ye, J. S. Du, X. Zhang, D. Kim, J. Loukusa, L. Ma, S. N. Ehrlich, N. S. Marinkovic, J. J. D. Yoreo, F. Liu, *Chem. Eng. J.* **2024**, *487*, 150486.
[2] W. Li, M. Zhang, X. Sun, C. Sheng, X. Mu, L. Wang, P. He, H. Zhou, *Nat. Commun.* **2024**, *15*, 803.
[3] X. Mu, P. He, H. Zhou, *Acc. Mater. Res.* **2024**, *5*, 467.
[4] X. Zhang, T. Luo, Y. Wang, Y. Li, *Chemistry* **2024**, *30*, e202400414.
[5] X. Zhang, Y. Wang, Y. Li, *Chem. Sci.* **2024**, *15*, 4804.
[6] L. Zhou, Y. Huang, Y. Wang, B. Wen, Z. Jiang, F. Li, *Nanoscale* **2024**, *16*, 17324.
[7] R. Mao, Y. Liu, P. Shu, B. Lu, B. Chen, Y. Chen, Y. Song, Y. Jia, Z. Zheng, Q. Peng, G. Zhou, *EcoMat* **2024**, *6*, e12449.
[8] H.-K. Lim, H.-D. Lim, K.-Y. Park, D.-H. Seo, H. Gwon, J. Hong, W. A. Goddard, H. Kim, K. Kang, *J. Am. Chem. Soc.* **2013**, *135*, 9733.
[9] B. Liu, Y. Sun, L. Liu, J. Chen, B. Yang, S. Xu, X. Yan, *Energy Environ. Sci.* **2019**, *12*, 887.
[10] Z. Xie, X. Zhang, Z. Zhang, Z. Zhou, *Adv. Mater.* **2017**, *29*, 1605891.
[11] Y. Qiao, J. Yi, S. Wu, Y. Liu, S. Yang, P. He, H. Zhou, *Joule* **2017**, *1*, 359.
[12] K. Xu, X.-C. Hu, C. Ma, P. Wang, W.-W. Wang, C.-J. Jia, *Catal. Sci. Technol.* **2023**, *13*, 6254.
[13] D. Wu, N. Tian, X. Sun, M. Wang, J. Huang, H. Deng, D. Yu, M. Wu, H. Ni, K. Pei, Y. Jia, P. Ye, *Mater. Chem. Phys.* **2021**, *258*, 123980.
[14] K. V. Savunthari, C. H. Chen, Y. R. Chen, Z. Tong, K. Iputera, F. M. Wang, C. C. Hsu, D. H. Wei, S. F. Hu, R. S. Liu, *ACS Appl. Mater. Interfaces* **2021**, *13*, 44266.
[15] H. Zhao, D. Li, H. Li, A. G. Tamirat, X. Song, Z. Zhang, Y. Wang, Z. Guo, L. Wang, S. Feng, *Electrochim. Acta* **2019**, *299*, 592.
[16] T. Jian, W. Ma, J. Hou, J. Ma, C. Xu, H. Liu, *Nano Energy* **2023**, *118*, 108998.
[17] Y. Liu, R. Mao, B. Chen, B. Lu, Z. Piao, Y. Song, G. Zhou, H.-M. Cheng, *Mater. Today* **2023**, *63*, 120.
[18] J. Zou, G. Liang, F. Zhang, S. Zhang, K. Davey, Z. Guo, *Adv. Mater.* **2023**, *35*, e2210671.
[19] G. Yue, X. Luo, Z. Hu, W. Xu, J. Li, J. Liu, R. Cao, *Chem. Commun.* **2020**, *56*, 11693.
[20] G. Yue, Z. Hong, Y. Xia, T. Yang, Y. Wu, *Coatings* **2022**, *12*, 1227.
[21] C. F. Wen, S. Yang, J. J. He, Q. Niu, P. F. Liu, H. G. Yang, *Small* **2024**, *20*, 2405051.
[22] K. Pobłocki, J. Drzeżdżon, B. Gawdzik, D. Jacewicz, *Green Chem.* **2022**, *24*, 9402.
[23] Y. P. Budiman, M. Rashifari, S. Azid, I. Z. Ghafara, Y. Deawati, Y. Permana, U. S. F. Arrozi, W. Ciptonugroho, T. Mayanti, W. W. Lestari, *ChemistrySelect* **2024**, *9*, e202304913.
[24] Y. Wu, H. Ding, T. Yang, Y. Xia, H. Zheng, Q. Wei, J. Han, D. L. Peng, G. Yue, *Adv. Sci.* **2022**, *9*, e2200523.
[25] R. Ballesteros-Garrido, R. Montagud-Martinez, G. Rodrigo, *ACS Appl. Mater. Interfaces* **2019**, *11*, 19878.
[26] T. Wang, H. Zhu, Q. Zeng, D. Liu, *Adv. Mater. Interfaces* **2019**, *6*, 1900423.
[27] P. G. Raje, S. R. Gurav, M. R. Waikar, A. S. Rasal, J.-Y. Chang, R. G. Sonkawade, *J. Energy Storage* **2022**, *56*, 105700.
[28] S. Jang, S. Jee, R. Kim, J. H. Lee, H. Y. Yoo, W. Park, J. Shin, K. M. Choi, *Bull. Korean Chem. Soc.* **2021**, *42*, 315.
[29] Z. Lian, Y. Lu, C. Wang, X. Zhu, S. Ma, Z. Li, Q. Liu, S. Zang, *Adv. Sci.* **2021**, *8*, 2102550.
[30] G. Zeng, Z. Yu, M. Du, N. Ai, W. Chen, Z. Gu, B. Chen, *ChemistrySelect* **2018**, *3*, 11601.
[31] K. M. Naik, A. K. Chourasia, M. Shavez, C. S. Sharma, *ChemSusChem* **2023**, *16*, e202300734.
[32] S.-M. Xu, Z.-C. Ren, X. Liu, X. Liang, K.-X. Wang, J.-S. Chen, *Energy Storage Mater.* **2018**, *15*, 291.
[33] L. Zhou, Z. Niu, X. Jin, L. Tang, L. Zhu, *ChemistrySelect* **2018**, *3*, 12865.
[34] J. Zhao, X. Xu, J. Chen, Y. Liu, J. Wu, F. Lou, Y. Fan, Y. Qiao, *J. Power Sources* **2024**, *607*, 234577.
[35] Y. Xia, T. Mao, X. Jin, L. Wang, J. Yan, S. Lin, D. L. Peng, Z. Yu, G. Yue, *J. Colloid. Interface Sci.* **2025**, *680*, 418.
[36] P. Pachfule, X. Yang, Q.-L. Zhu, N. Tsumori, T. Uchida, Q. Xu, *J. Mater. Chem. A* **2017**, *5*, 4835.
[37] W. Xie, C. Shi, H. Li, L. Liu, Y. Zhao, C. Lin, *ACS Appl. Nano Mater.* **2024**, *7*, 3210.
[38] X. Ye, W. Liu, Y. Lu, X. Zheng, Y. Bi, M. Zheng, L. Han, B. Liu, Y. Ning, S. H. M. Jafri, X. Zhao, S. He, S. Zhang, H. Li, *J. Mater. Chem. A* **2024**, *12*, 10713.
[39] T. Yang, Y. Xia, T. Mao, Q. Ding, Z. Wang, Z. Hong, J. Han, D. L. Peng, G. Yue, *Adv. Funct. Mater.* **2022**, *32*, 22098762.
[40] S. Jing, M. Zhang, H. Liang, B. Shen, S. Yin, X. Yang, *J. Mater. Sci.* **2017**, *53*, 4395.
[41] Z. Zhang, C. Yang, S. Wu, A. Wang, L. Zhao, D. Zhai, B. Ren, K. Cao, Z. Zhou, *Adv. Energy Mater.* **2019**, *9*, 1802805.
[42] P.-F. Zhang, Y.-Q. Lu, Y.-J. Wu, Z.-W. Yin, J.-T. Li, Y. Zhou, Y.-H. Hong, Y.-Y. Li, L. Huang, S.-G. Sun, *Chem. Eng. J.* **2019**, *363*, 224.
[43] H. Liang, Y. Zhang, F. Chen, S. Jing, S. Yin, P. Tsiakaras, *Appl. Catal. B* **2019**, *244*, 559.
[44] X. Li, H. Wang, Z. Chen, H. S. Xu, W. Yu, C. Liu, X. Wang, K. Zhang, K. Xie, K. P. Loh, *Adv. Mater.* **2019**, *31*, e1905879.
[45] Z. Guo, J. Li, H. Qi, X. Sun, H. Li, A. G. Tamirat, J. Liu, Y. Wang, L. Wang, *Small* **2019**, *15*, e1803246.
[46] Y. C. Tan, H. C. Zeng, *Adv. Funct. Mater.* **2017**, *27*, 1703765.

Manuscript received: April 20, 2025
Revised manuscript received: May 20, 2025
Version of record online: